ACS Photonics

Article

Cite This: ACS Photonics XXXX, XXX, XXX−XXX

Terahertz Magnon-Polaritons in $TmFeO_3$

Kirill Grishunin,[†] Thomas Huisman,[‡] Guanqiao Li,[‡] Elena Mishina,[†] Theo Rasing,[‡] Alexey V. Kimel,[†,‡] Kailing Zhang,[§] Zuanming Jin,[§] Shixun Cao,[§] Wei Ren,[§] Guo-Hong Ma,*[,§] and Rostislav V. Mikhaylovskiy*[,‡]

[†]Moscow Technological University (MIREA), Moscow, Russia

[‡]Radboud University, Institute for Molecules and Materials, Nijmegen, The Netherlands

[§]Department of Physics, Shanghai University, Shanghai, China

ABSTRACT: Magnon-polaritons are shown to play a dominant role in the propagation of terahertz (THz) waves through $TmFeO_3$ orthoferrite, if the frequencies of the waves are in the vicinity of the quasi-antiferromagnetic spin resonance mode. Both time-domain THz transmission and emission spectroscopies reveal clear beatings between two modes with frequencies slightly above and slightly below this resonance, respectively. Rigorous modeling of the interaction between the spins of $TmFeO_3$ and the THz light shows that the frequencies correspond to the upper and lower magnon-polariton branches. Our findings reveal the previously ignored importance of propagation effects and polaritons in such heavily debated areas as THz magnonics and THz spectroscopy of electromagnons. It also shows that future progress in these areas calls for an interdisciplinary approach at the interface between magnetism and photonics.

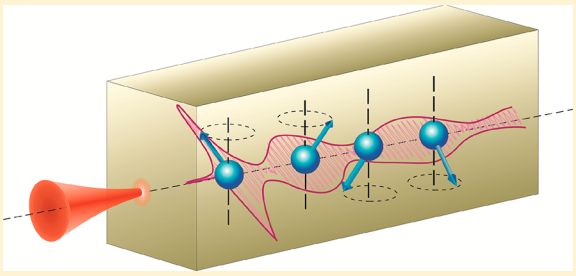

KEYWORDS: *polaritonics, magnonics, terahertz spectroscopy, antiferromagnetism, ultrafast dynamics*

Photonics and magnonics appeal to information technologies for their potential to overcome the problems inherent to modern electronics, such as dissipation of energy due to Ohmic losses.[1−4] The viability of magnonics depends on a successful increase of the frequency of magnon-based processing, which in traditional ferromagnetic materials (e.g., YIG) is restricted to the GHz regime.[5−7] The use of antiferromagnetic materials could be a solution because of their very high (terahertz) frequencies of spin resonances.[8,9] However, the physics of magnons at THz frequencies is far less studied due to a lack of sufficiently fast stimuli and detectors in this area. This therefore calls for an interdisciplinary approach at the intersection of magnetism and photonics. For example, the latest advances in the development of strong THz field sources have opened a doorway for coherent control over magnetism at ultrashort time scales.[10]

Here we report an experimental and theoretical study of antiferromagnetic magnon-polariton propagation in the orthoferrite $TmFeO_3$. For this, we employ THz transmission and emission time-domain spectroscopy. Our experimental findings are supported by a rigorous solution of the Maxwell equations.

The rare-earth orthoferrites R-FeO_3 offer plenty of opportunities for this type of research. $TmFeO_3$ has been extensively used as a model system to investigate ultrafast spin dynamics.[11−13] This particular orthoferrite has numerous resonances in the THz frequency range related to magnetic resonances of the iron sublattices and electronic transitions in the Tm ions.[14,15]

Figure 1a shows the unit-cell of the $TmFeO_3$ single crystal, taking into account the parameter from refs.[16,17] The compound crystallizes in the *Pbnm* structural phase. The spins of Fe^{3+} ions are ordered antiferromagnetically. The magnetic structure can be described by four magnetic sublattices with the magnetizations $\mathbf{M}_1$, $\mathbf{M}_2$, $\mathbf{M}_3$, and $\mathbf{M}_4$, respectively. Owing to the Dzyaloshinsky-Moriya interaction, the antiferromagnetic Fe^{3+} spins are canted over a small angle from the antiparallel orientation and give rise to a net magnetization $\mathbf{M} = \mathbf{M}_1 + \mathbf{M}_2 + \mathbf{M}_3 + \mathbf{M}_4$. Such a magnetic structure has two spin resonance modes, namely the quasi-ferromagnetic mode (F-mode) and the quasi-antiferromagnetic mode (AF-mode).[18] For $TmFeO_3$, both these modes are in the THz spectral range. The F-mode resonance can be seen as a precession of the macroscopic magnetization $\mathbf{M}$. The AF-mode, on the other hand, can be seen as a longitudinal oscillation of the magnetization $\mathbf{M}$ due to the canting of the Fe^{3+} spins induced by the Dzyaloshinksy-Moriya interaction.[13,19]

The single crystals of $TmFeO_3$ studied here were grown in a four-mirror optical floating-zone furnace using four 1.5 kW halogen lamps as the infrared radiation source. The samples had a thickness of about 1.5 mm and were oriented by using X-ray Laue photography. X-ray Laue analysis and X-ray diffraction rocking curves confirmed the high quality, precise orientation, and homogeneity of the studied crystals.

Received: November 21, 2017
Published: February 1, 2018

DOI: 10.1021/acsphotonics.7b01402
ACS Photonics XXXX, XXX, XXX−XXX

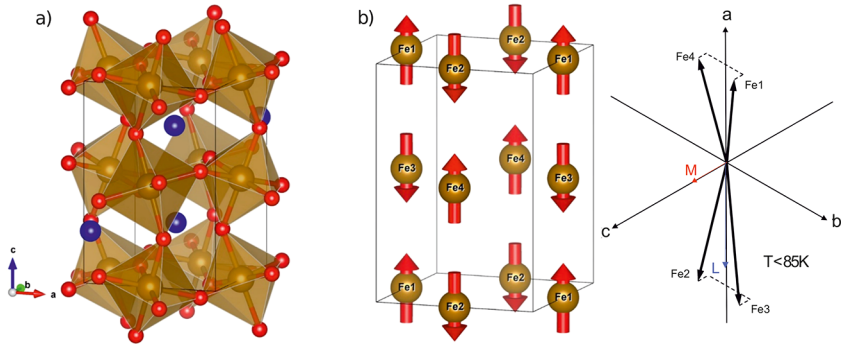

Figure 1. (a) Crystal structure of a $TmFeO_3$ crystal (blue, thulium; brown, iron; red, oxygen). Fe ions are located in centrosymmetrical positions having a distorted octahedral oxygen environment; (b) Spin alignment of the four antiferromagnetic Fe^{3+} sublattices in the Γ_2 phase below 80 K.

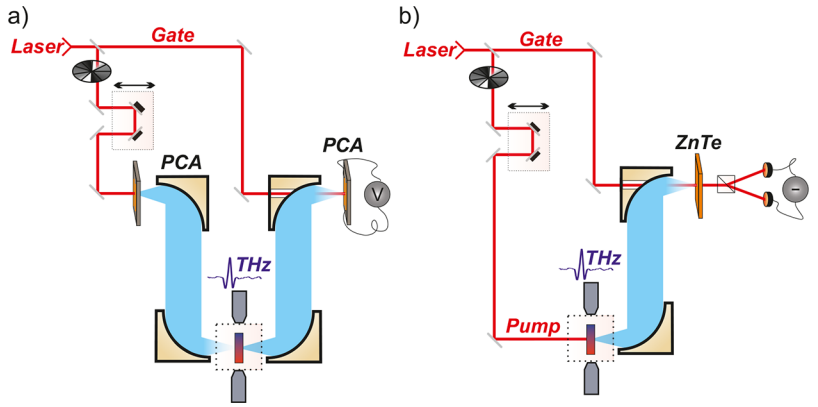

Figure 2. Schematics of experimental setups. (a) Time-domain THz transmission spectroscopy (TDS). Photoconductive antennas (PCA), fabricated on low-temperature-grown GaAs substrates, were used for the generation and detection of the THz radiation; (b) THz emission spectroscopy. The THz waves were emitted from the sample illuminated by an intense femtosecond laser pulse. The detection of the THz radiation involved ZnTe electro-optical crystals and polarization balanced detection.

The magnetic anisotropy of $TmFeO_3$ undergoes dramatic changes as a function of temperature and the compound is characterized by a so-called spin reorientation transition in which the net magnetization changes its orientation.[20,21] In our sample at higher temperatures (T > 93 K), the spins are in the Γ_4 phase, with the net magnetization $\mathbf{M}$ along the c-axis and the antiferromagnetic vector $\mathbf{L} = \mathbf{M}_1 - \mathbf{M}_2 + \mathbf{M}_3 - \mathbf{M}_4$ along the a-axis. At lower temperatures (T < 85 K), the spins are in the Γ_2 phase with the magnetization and antiferromagnetic vectors along the a and c axes, respectively. In the region between 85 and 93 K, there is an intermediate phase Γ_{24} in which the antiferromagnetic and magnetization vectors rotates continuously in the ac plane.[22]

To reveal the strong coupling between the photons and magnons we have performed two types of experiments. The first one was transmission THz time-domain spectroscopy (THz-TDS). The corresponding experimental scheme is shown in Figure 2a. The output of a mode-locked Ti:Sapphire laser with pulse duration of 100 fs, centered wavelength of 800 nm, and repetition rate of 80 MHz (Mai Tai HP-1020, Spectra-Physics) was used to generate and detect the THz transients. The emitter and detector of the THz waves were photoconductive antennas (PCA) fabricated on low-temperature-grown GaAs substrates.

The second type of experiment was THz emission spectroscopy (Figure 2b). In this technique the sample was illuminated by a femtosecond laser pulse (estimated duration of ~50 fs, central wavelength of 680 nm, and repetition rate of 1 kHz) and served as an emitter of THz radiation. The THz radiation emitted from the sample was focused onto the 1 mm thick [110] ZnTe electro-optic crystal gated by femtosecond laser pulses at 800 nm. The terahertz-induced changes of the linear polarization of the gating pulses in the electro-optic crystal were analyzed by polarization optics consisting of a quarter-wave plate, a Wollaston polarizer and a pair of balanced silicon photodiodes. To increase the signal-to-noise ratio, we used an opto-mechanical chopper modulating the pump beam intensity combined with a lock-in amplifier.

In all these experiments the sample was placed in a coldfinger cryostat with two transparent windows and biased by in-plane magnetic fields with a strength up to 1 kG. Furthermore, the THz spectrometer and THz emission setup were purged with nitrogen in order to minimize absorption of THz radiation by atmospheric water vapor.

THz-TDS allows us to measure the free-induction decay (FID) signals, which result from the magnetic dipole transitions in the THz frequency range. The propagation direction of incident pulses was coaligned with the c-axis and the magnetic component of the pulse was pointed along the a-axis of the crystal ($\mathbf{B}_{THz} \| a$).

Figure 3a shows typical waveforms of the THz electrical field transmitted through the $TmFeO_3$ crystal at various temperatures. Below 90 K in the Γ_2 phase, the main transmitted THz pulse is followed by a long-lived and damped harmonic oscillation component at a frequency around 0.86 THz. Upon temperature decrease the frequency of the oscillations does not

DOI: 10.1021/acsphotonics.7b01402
ACS Photonics XXXX, XXX, XXX−XXX

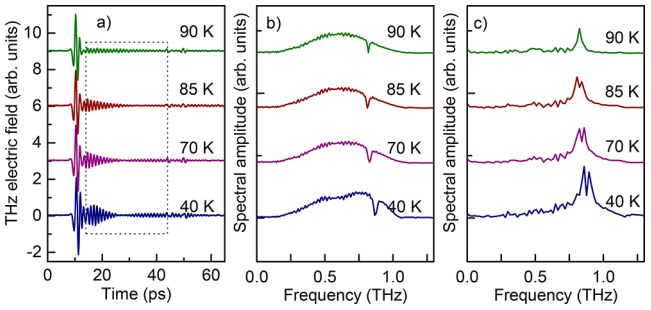

Figure 3. (a) Time-domain trances of the electric field of THz pulses transmitted through $TmFeO_3$ single crystal for different temperatures; Fourier transforms of the time-domain traces (b) for all range and (c) for the area marked with a rectangle, the region between the THz pulse and its echo (from 14 to 45 ps).

change, while the amplitude increases. Above 90 K, the oscillations disappear completely. The frequency corresponds to the quasi-antiferromagnetic (AF-mode) in this material.[23] In the present geometry it can only be excited by a THz magnetic field in the Γ_2 phase. In the Fourier spectra in Figure 3b, this mode is seen as a narrow resonance dip at a frequency of about 0.86 THz; energy from the THz pulses is transferred to the excitation of the AF-mode, which subsequently re-emits part of this energy.

Despite the fact that there is only a single dip observed in the Fourier spectrum for all time-domain range, the changing envelope in the amplitude of the oscillations in the time-domain traces and Fourier transforms for the region between the THz pulse and its echo (Figure 3a) and the corresponding spectra (Figure 3c) indicate beating between two close frequencies.

In the second experiment, a femtosecond laser pulse with a photon energy of 1.82 eV (wavelength 680 nm) generates THz emission from the excited crystal. Figure 4a shows the time-

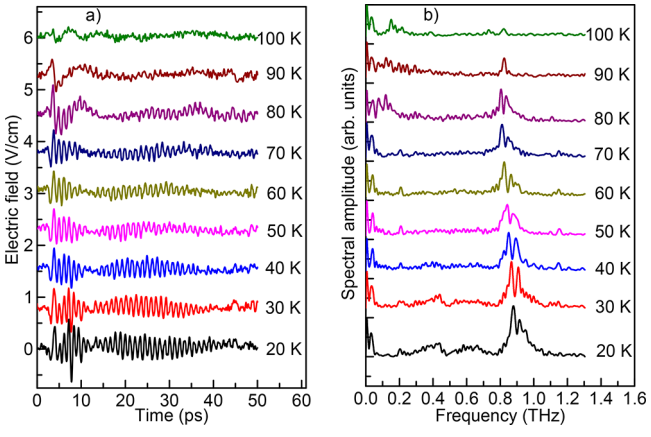

Figure 4. (a) Time traces of the electric field of the THz radiation emitted from a $TmFeO_3$ single crystal at different temperatures; (b) Fourier transforms of the time-domain emission waveforms.

traces of the THz electric field emitted from the $TmFeO_3$ crystal at various temperatures. The emitted radiation contains quasi-monochromatic oscillations with beatings. The amplitude of the observed oscillations decreases upon temperature increase and vanishes in the Γ_4 phase (T > 90 K). The frequency spectra of the time-domain emission signals (Figure 4b) show two distinguishable peaks at frequencies just below and above the frequency of the AF-mode of the antiferromagnetic resonance in the Γ_2 phase of $TmFeO_3$.

To understand the physical origin of the beatings we derived a model of light−matter interaction in the THz spectral range.

MODELS

Terahertz Transmission. As the THz spot on the sample is large compared to the THz wavelength, we employ a plane-wave approximation, assuming that the wave vector **k** of the electromagnetic waves is perpendicular to the interface. It means that the waves propagate along the z-axis, which is the c-axis of $TmFeO_3$. The electric **E** and the magnetic field **B** vectors are directed along the x- and y-axes, respectively (Figure 5a).

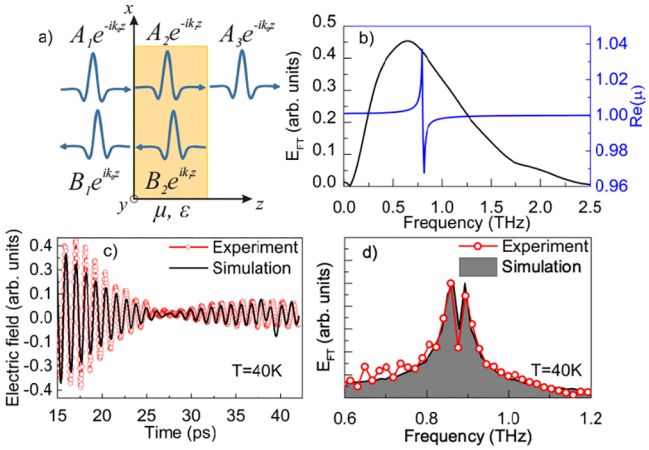

Figure 5. (a) Geometry of the THz transmission experiment and electromagnetic waves relevant to the problem of light-matter interaction; (b) Spectrum of the THz pulse and frequency-dependence of the real part of the $TmFeO_3$ magnetic permeability $\mu(\omega)$; (c) Comparison of calculated and measured (at T = 40 K) THz waveforms transmitted through the $TmFeO_3$ sample for the region between the THz pulse and its echo; (d) Fourier transforms of the time traces shown in panel (c).

To find the THz radiation transmitted through an infinite plate of thickness d with relative permittivity ε and magnetic permeability $\mu = \mu(\omega)$, we use the wave equation in the frequency domain. In Gaussian units it gives

$$\frac{\partial}{\partial z}\left(\frac{1}{\mu(z,\omega)}\frac{\partial \tilde{E}_x}{\partial z}\right) + \frac{\omega^2}{c^2}\varepsilon(z)\tilde{E}_x = 0 \quad (1)$$

where the wavy line symbol is used to indicate the Fourier transform with respect to time.

The solution has the form of plane waves:

$$\tilde{E}_x(z) = \begin{cases} A_1 e^{-ik_0 z} + B_1 e^{ik_0 z}, & z < 0 \\ A_2 e^{-ik_1 z} + B_2 e^{ik_1 z}, & 0 < z < d \\ A_3 e^{-ik_0 z}, & d < z \end{cases} \quad (2)$$

where A_i and B_i are the amplitudes of the transmitted and reflected electromagnetic waves, k_0 is the wave vector in air, k_1 is the wave vector in the material, and d is the thickness of the sample.

From Faraday's law, the electric field $\tilde{E}_x$ should be continuous at the interfaces. Furthermore, by integrating eq 1 along an infinitesimal interval Δz we come to the boundary

DOI: 10.1021/acsphotonics.7b01402
ACS Photonics XXXX, XXX, XXX−XXX

conditions of continuity of $\left(\frac{1}{\mu}\frac{\partial \tilde{E}_x}{\partial z}\right)$. These requirements provide the following set of equations:

$$z=0:\begin{cases} A_1+B_1=A_2+B_2, \\ -k_0A_1+k_0B_1=-\dfrac{k_1}{\mu(\omega)}A_2+\dfrac{k_1}{\mu(\omega)}B_2, \end{cases}$$

$$z=d:\begin{cases} A_2e^{-ik_1d}+B_2e^{ik_1d}=A_3e^{-ik_0d}, \\ -\dfrac{k_1}{\mu(\omega)}A_2e^{-ik_1d}+\dfrac{k_1}{\mu(\omega)}B_2e^{ik_1d}=-k_0A_3e^{-ik_0d} \end{cases} \tag{3}$$

Solving this set of equations for A_3, we obtain a solution for the ratio between the spectrum of light transmitted through the slab and the incident spectrum:

$$t(\omega)=\frac{A_3}{A_1}E(\omega)=\frac{-4k_0k_1\mu(\omega)e^{-ik_1d}}{(k_1-k_0\mu(\omega))^2e^{-ik_1d}-(k_1+k_0\mu(\omega))^2e^{ik_1d}}E(\omega) \tag{4}$$

where $E(\omega)$ is the normalized spectrum amplitude of the incident THz pulse.

One expects to see manifestations of magnetic modes in transmission due to singularities of the magnetic permeability in the vicinity of resonances. For the permeability of the material, we used the standard Drude-Lorentz form (Figure 5b):

$$\mu(\omega)=\frac{\Delta\mu\omega_0^2}{\omega_0^2-\omega^2-i\omega\Delta\omega} \tag{5}$$

with the resonant frequency ω_0, absorption line width $\Delta\omega$, and the effective oscillator strength $\Delta\mu$.

Taking ω_0 = 860 GHz for the resonant frequency, the sample thickness d = 1.5 mm, tabulated values for other parameters ($\Delta\omega$ = 8.6 GHz, $\Delta\mu = 10^{-3}$, $\varepsilon = 22-0.26i$)[23] and the spectrum of the incident THz pulse we applied inverse Fourier transformation to eq 5. As a result, we obtained a time-domain profile of the electric field for the radiation transmitted through the structure (Figure 5c) and its spectrum (Figure 5d).

The outcome of the model appears to be in very good agreement with the experimental data.

Terahertz Emission. As demonstrated in previous works,[13,23] femtosecond laser excitation can effectively excite the AF-mode of magnetic resonance in $TmFeO_3$ due to a photoinduced change of the ratio between the exchange parameters in the canted antiferromagnet. This action of the laser pulse on spins can be described as a pulse of an effective magnetic field $\mathbf{H}_{\text{eff}}$ along the magnetization $\mathbf{M}$. To find the THz radiation triggered by such an effective field, we solve the Maxwell equations in the frequency domain:

$$\nabla\times\tilde{\mathbf{E}}=\frac{i\omega\mu(\omega)}{c}\tilde{\mathbf{H}} \tag{6}$$

$$\nabla\times\tilde{\mathbf{H}}=-\frac{i\omega\varepsilon}{c}\tilde{\mathbf{E}}-4\pi i\omega(\nabla\times\tilde{\mathbf{M}}) \tag{7}$$

where $\tilde{\mathbf{M}}=\chi(\omega)\tilde{\mathbf{H}}_{\text{eff}}$ and $\chi(\omega)$ is the magnetic susceptibility.

Dividing eq 6 by $\mu(\omega)$, taking the curl of the cross product $\nabla\times\tilde{\mathbf{E}}$ and using eq 7 we obtain

$$\nabla\times\left(\frac{1}{\mu(\omega)}\nabla\times\tilde{\mathbf{E}}\right)+\frac{\omega^2\varepsilon}{c^2}\tilde{\mathbf{E}}=-\frac{4\pi\omega^2}{c\mu(\omega)}(\nabla\times\tilde{\mathbf{M}}) \tag{8}$$

This simplifies to

$$\mu(\omega)\frac{\partial}{\partial z}\left(\frac{1}{\mu(\omega)}\frac{\partial\tilde{E}_x}{\partial z}\right)+k^2\tilde{E}_x=-\frac{4\pi\omega^2}{c\mu(\omega)}\frac{\partial(\chi(\omega)\tilde{H}_{\text{eff}})}{\partial z} \tag{9}$$

where $k=\frac{\omega}{c}\sqrt{\varepsilon\mu(\omega)}$ is the wave vector.

The effective magnetic field $\tilde{H}_{\text{eff}}$ follows the intensity envelope of the optical Gaussian pump pulse.[25] The propagation speed of this pulse is v_{gr}, the penetration depth into the material is l. In the frequency domain, this can be represented as

$$\tilde{H}_{\text{eff}}=f(\omega)e^{-i\omega z/v_{\text{gr}}}e^{-z/l} \tag{10}$$

where $f(\omega)=A_0\frac{\tau_p}{\sqrt{2\pi}}e^{-\omega^2\tau_p{}^2/4}$ is the spectrum of the envelope of the optical intensity, τ_p is the pulse duration, A_0 is the spectral amplitude of the effective magnetic field.

The solution of eq 9 has the form

$$\tilde{E}_x(z)=\begin{cases} B_1e^{ik_0z}, & z<0 \\ A_2e^{-ik_1z}+B_2e^{ik_1z}+U(z), & 0<z<d \\ A_3e^{-ik_0z}, & d<z \end{cases} \tag{11}$$

where $U(z)$ is a partial solution, k_0 is the wave vector in air, k_1 is the wave vector in the material, and d is the thickness of the sample.

Taking the partial solution in the form $U(z)=G(\omega)e^{-i\omega z/v_{\text{gr}}}e^{-z/l}$,[25] it is found from eq 9 that

$$U(z)=-\frac{4\pi i\omega\alpha\chi(\omega)}{c(\alpha^2-k^2)}\tilde{H}_{\text{eff}}(z) \tag{12}$$

where $\alpha=\frac{i\omega}{v_{\text{gr}}}+\frac{1}{l}$ is the effective optical penetration decay.

By integrating Maxwell's equations over an infinitesimal length crossing the interfaces and taking the limit as the thicknesses of the transition regions go to zero, one gets the boundary conditions. These boundary-matching conditions imply continuity of the electric field, while its derivative exhibits a finite discontinuity:

$$\{\tilde{E}_x\}=0,$$

$$\left\{\frac{1}{\mu(\omega)}\frac{\partial\tilde{E}_x}{\partial z}\right\}=\pm\frac{4\pi\omega^2\chi(\omega)}{c\mu(\omega)}\tilde{H}_{\text{eff}}$$

These requirements provide the following system of equations:

$$z=0:\begin{cases} B_1=A_2+B_2+U(0), \\ ik_0B_1=\dfrac{ik_1}{\mu(\omega)}A_2-\dfrac{ik_1}{\mu(\omega)}B_2-\dfrac{\alpha}{\mu(\omega)}U(0), \end{cases}$$

$$z=d:\begin{cases} A_2e^{ik_1d}+B_2e^{-ik_1d}+U(d)=A_3e^{-ik_0d}, \\ \dfrac{ik_1}{\mu(\omega)}A_2e^{ik_1d}-\dfrac{ik_1}{\mu(\omega)}B_2e^{-ik_1d}+\dfrac{\alpha}{\mu(\omega)}U(d) \\ \quad=-ik_0A_3e^{-ik_0d} \end{cases} \tag{13}$$

Solving these equations for A_3, we obtain the solution for the spectrum of the THz radiation emitted from the slab:

DOI: 10.1021/acsphotonics.7b01402
ACS Photonics XXXX, XXX, XXX−XXX

$$A_3 = \left[e^{-\alpha d}U(\omega)(\gamma(1-i\xi)(-2e^{(\alpha+ik_1)d}+e^{2ik_1d}+1)+\gamma^2(-1+e^{2ik_1d}) - i\xi(-1+e^{2ik_1d}))\right]/[(\gamma+1)^2e^{2ik_1d}-(\gamma-1)^2] \quad (14)$$

where $\gamma = \gamma(\mu, \omega) = k_1(\mu, \omega)/k_0(\omega)$ and $\xi(\omega) = -\alpha(\omega)/k_0(\omega)$ are introduced to simplify the expression.

Figure 6 shows such a spectrum (Figure 6b) and the corresponding waveform (Figure 6c). For the calculation we used $v_{gr} = c/n$, $n = 2.3$ at $\lambda = 680$ nm; $l = 50$ μm,[26] and $\tau_p = 50$. It is seen that the model is in good agreement with the outcome of the experiment.

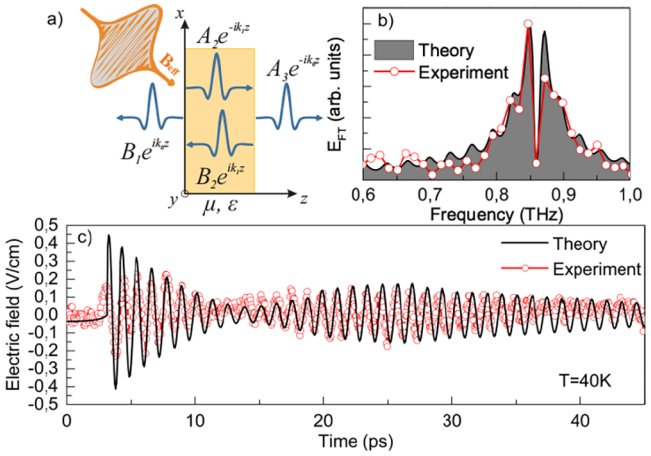

Figure 6. (a) Geometry of THz generation in a slab of orthoferrite and the electromagnetic waves relevant to the problem of light−matter interaction; (b) Calculated and measured Fourier amplitudes E_{FT} of the electric field for radiation generated in the $TmFeO_3$ sample slab by a laser pulse at 40 K; (c) The time traces corresponding to the spectra shown in (b).

DISCUSSION

We would like to note that, although our models do not contain fitting parameters, they correctly predict the bandwidth of the THz spectrum, position of the beat frequencies, and the positions of the Fabry−Perot peaks.

The dispersion of photons ($k(\omega)$ dependence from eq 9) in the absence of magnetic resonances ($\mu(\omega) = \text{const}$) is a linear function (Figure 7, black line). In the presence of a spin resonance ($\mu(\omega) \neq \text{const}$) without spatial dispersion, the $\omega(k)$ curve has an avoided crossing at the resonance frequency (Figure 7, dash line). However, taking into account dissipation of the magnetic permeability, one finds that a coupled photon-magnon (polariton) is formed (Figure 7, blue solid line). In the vicinity of the resonance frequency for each wave vector there are two allowed modes that satisfy the dispersion equation and have positive dispersion (Figure 7, red points). An excitation by THz or femtosecond laser pulses excites two polariton modes with close frequencies, which are seen as beatings in time-resolved experiments.

As the magnon-polaritons propagate in space it is instructive to analyze their beating as a function of the crystal thickness. In Figure 8 we show the beating spectra for both THz transmission (Figure 8a) and emission (Figure 8b), calculated for different thicknesses of the sample. As one can see from the figure, as the crystal becomes thicker the beating is more pronounced. Also, in the case of transmission, the polariton beating interferes with the Fabry−Perot echoes of the broadband THz pulse for thicknesses less than 1 mm, which further hinders the observation of beatings in this type of measurement. This analysis is in line with the absence of a clear beating in previous experiments [e.g., refs 13, 22, 24], in which much thinner crystals with thicknesses less than 200 μm were studied.

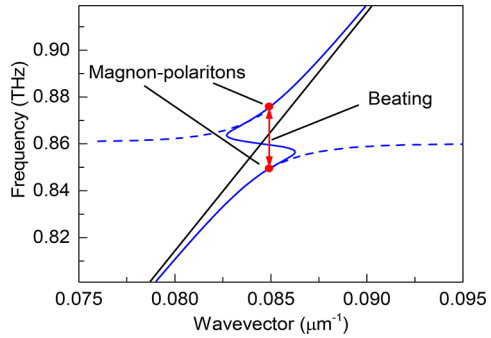

Figure 7. Magnon-polariton dispersion in the vicinity of a spin resonance (blue dashed line for an ideal system, infinite discontinuity; blue solid line for the real $TmFeO_3$). The linear dispersion of photons in the absence of the spin resonance is shown for comparison (black line). In the vicinity of the resonance frequency for each wave vector, one would get not one, but two solutions corresponding to two magnon-polaritons (red circles) at close frequencies.

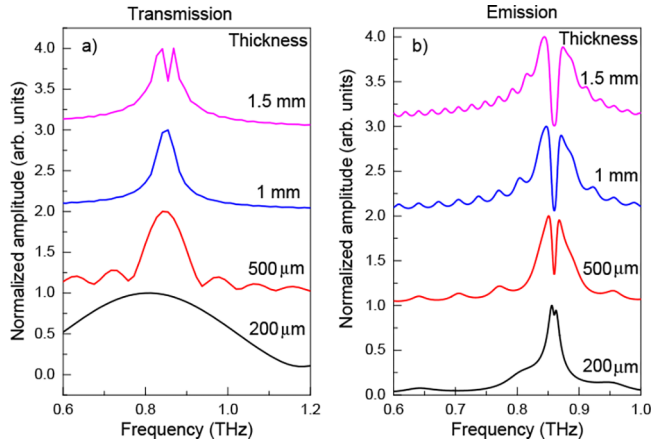

Figure 8. (a) Calculated transmission beating spectra for the region between the THz pulse and its echo in the time-domain range for different crystal thicknesses; (b) emission spectra for different crystal thicknesses.

CONCLUSIONS

Time-domain spectroscopy of THz magnetic resonances in orthoferrites shows that the observed spectra cannot be described without accounting for propagation of electromagnetic waves. Instead of a single peak in the spectra, two peaks with frequencies slightly below and slightly above the frequency of the magnetic resonance are observed. Our findings have implications for several other areas of physics including THz magnonics[27] and spectroscopy of electromagnons.[28] Therefore, further progress in these areas calls for an interdisciplinary approach at the interface between magnetism and photonics.

DOI: 10.1021/acsphotonics.7b01402
ACS Photonics XXXX, XXX, XXX−XXX

AUTHOR INFORMATION

Corresponding Authors

*E-mail: ghma@staff.shu.edu.cn.
*E-mail: r.mikhaylovskiy@science.ru.nl.

ORCID

Kirill Grishunin: 0000-0001-9523-355X
Wei Ren: 0000-0001-7317-3867
Guo-Hong Ma: 0000-0002-3972-5012

Notes

The authors declare no competing financial interest.

ACKNOWLEDGMENTS

This work is supported by the National Natural Science Foundation of China (NSFC, Nos. 11674213, 11604202, 61735010 and 51372149), the European Research Council ERC Grant Agreement No. 339813 (Exchange) and NWO (The Netherlands Organization for Scientific Research). Z. J. thanks the Young Eastern Scholar (QD2015020) at Shanghai Institutions of Higher Learning. Universities Young Teachers Training Funding Program (ZZSD15098) and "Chen Guang" project (16CG45). K.A.G., E.D.M., A.V.K. thanks the Russian Science Foundation (16-12-10520) and the Ministry of Education and Science of the Russian Federation (contract no. 14.Z50.31.0034).

REFERENCES

(1) Kruglyak, V. V.; Demokritov, S. O.; Grundler, D. Magnonics. *J. Phys. D: Appl. Phys.* **2010**, *43* (26), 264001.
(2) Lenk, B.; Ulrichs, H.; Garbs, F.; Munzenberg, M. The Building Blocks of Magnonics. *Phys. Rep.* **2011**, *507*, 107−136.
(3) Locatelli, N.; Cros, V.; Grollier, J. Spin-Torque Building Blocks. *Nat. Mater.* **2014**, *13* (1), 11−20.
(4) Divinskiy, B.; Demidov, V. E.; Demokritov, S. O.; Rinkevich, A. B.; Urazhdin, S. Route toward High-Speed Nano-Magnonics Provided by Pure Spin Currents. *Appl. Phys. Lett.* **2016**, *109* (25), 252401.
(5) Serga, A. A.; Chumak, A. V.; Hillebrands, B. YIG Magnonics. *J. Phys. D: Appl. Phys.* **2010**, *43* (26), 264002.
(6) Liu, X.; Zhang, W.; Carter, M. J.; Xiao, G. Ferromagnetic Resonance and Damping Properties of CoFeB Thin Films as Free Layers in MgO-Based Magnetic Tunnel Junctions. *J. Appl. Phys.* **2011**, *110* (3), 33910.
(7) Lee, S.; Grudichak, S.; Sklenar, J.; Tsai, C. C.; Jang, M.; Yang, Q.; Zhang, H.; Ketterson, J. B. Ferromagnetic Resonance of a YIG Film in the Low Frequency Regime. *J. Appl. Phys.* **2016**, *120* (3), 33905.
(8) Kampfrath, T.; Sell, A.; Klatt, G.; Pashkin, A.; Mährlein, S.; Dekorsy, T.; Wolf, M.; Fiebig, M.; Leitenstorfer, A.; Huber, R. Coherent Terahertz Control of Antiferromagnetic Spin Waves. *Nat. Photonics* **2010**, *5* (1), 31−34.
(9) Jungwirth, T.; Marti, X.; Wadley, P.; Wunderlich, J. Antiferromagnetic Spintronics. *Nat. Nanotechnol.* **2016**, *11* (3), 231−241.
(10) Kampfrath, T.; Tanaka, K.; Nelson, K. a. Resonant and Nonresonant Control over Matter and Light by Intense Terahertz Transients. *Nat. Photonics* **2013**, *7* (9), 680−690.
(11) Kimel, A. V.; Kirilyuk, A.; Tsvetkov, A.; Pisarev, R. V.; Rasing, T. Laser-Induced Ultrafast Spin Reorientation in the Antiferromagnet $TmFeO_3$. *Nature* **2004**, *429* (6994), 850−853.
(12) Kimel, A. V.; Stanciu, C. D.; Usachev, P. A.; Pisarev, R. V.; Gridnev, V. N.; Kirilyuk, A.; Rasing, T. Optical Excitation of Antiferromagnetic Resonance in $TmFeO_3$. *Phys. Rev. B: Condens. Matter Mater. Phys.* **2006**, *74* (6), 60403.
(13) Mikhaylovskiy, R. V.; Hendry, E.; Secchi, A.; Mentink, J. H.; Eckstein, M.; Wu, A.; Pisarev, R. V.; Kruglyak, V. V.; Katsnelson, M. I.; Rasing, T.; Kimel, A. V. Ultrafast Optical Modification of Exchange Interactions in Iron Oxides. *Nat. Commun.* **2015**, *6*, 8190.
(14) Venugopalan, S.; Dutta, M.; Ramdas, A. K.; Remeika, J. P. Raman Scattering Study of Magnons at the Spin-Reorientation Transitions of $TbFeO_3$ and $TmFeO_3$. *Phys. Rev. B: Condens. Matter Mater. Phys.* **1983**, *27* (5), 3115−3118.
(15) Kozlov, G. V.; Mukhin, A. A.; Pronin, A. Y.; Prokhorov, A. S.; Zelezny, V.; Petzelt, J. Observation of Magnetic Dipole and Electric Dipole Electron Transitions in the Ground Multiplet of the Rare-Earth Ion in $TmFeO_3$. *Phys. Lett. A* **1990**, *52* (5), 264.
(16) Marezio, M.; Remeika, J. P.; Dernier, P. D. The Crystal Chemistry of the Rare Earth Orthoferrites. *Acta Crystallogr., Sect. B: Struct. Crystallogr. Cryst. Chem.* **1970**, *26* (12), 2008−2022.
(17) Aleksovska, S.; Dimitrovska, S.; Kuzmanovski, I. Crystal Structure Prediction in Orthorhombic ABO_3 Perovskites by Multiple Linear Regression and Artificial Neural Networks. *Acta Chim. Slov.* **2007**, *54* (3), 574−582.
(18) Herrmann, G. F. Magnetic Resonances and Susceptibility in Orthoferrites. *Phys. Rev.* **1964**, *133* (5A), A1334−A1344.
(19) Fu, X.; Liu, X.; Zhou, J. Terahertz Spectroscopic Observation of Spin Reorientation Induced Antiferromagnetic Mode Softening in $DyFeO_3$ Ceramics. *Mater. Lett.* **2014**, *132*, 190−192.
(20) White, R. L. Review of Recent Work on the Magnetic and Spectroscopic Properties of the Rare-Earth Orthoferrites. *J. Appl. Phys.* **1969**, *40* (3), 1061−1069.
(21) Belov, K. P.; Volkov, R. A.; Goranskii, B. P.; Kadomtseva, A. M.; Uskov, V. V. Nature of the Transitions during the Spontaneous Reorientation of Spins in Rare-Earth Orthoferrites. *Sov. Phys. Solid State* **1969**, *11*, 935−938.
(22) Baierl, S.; Hohenleutner, M.; Kampfrath, T.; Zvezdin, A. K.; Kimel, A. V.; Huber, R.; Mikhaylovskiy, R. V. Nonlinear Spin Control by Terahertz-Driven Anisotropy Fields. *Nat. Photonics* **2016**, *10* (11), 715−718.
(23) Mikhaylovskiy, R. V.; Hendry, E.; Kruglyak, V. V.; Pisarev, R. V.; Rasing, T.; Kimel, A. V. Terahertz Emission Spectroscopy of Laser-Induced Spin Dynamics in $TmFeO_3$ and $ErFeO_3$ Orthoferrites. *Phys. Rev. B: Condens. Matter Mater. Phys.* **2014**, *90* (18), na.
(24) Srinivasan, G.; Slavin, A. N. *High Frequency Processes in Magnetic Materials*; World Scientific, 1995.
(25) Mikhaylovskiy, R. V.; Huisman, T. J.; Popov, A. I.; Zvezdin, A. K.; Rasing, T.; Pisarev, R. V.; Kimel, A. V. Terahertz Magnetization Dynamics Induced by Femtosecond Resonant Pumping of Dy3+ Subsystem in the Multisublattice Antiferromagnet $DyFeO_3$. *Phys. Rev. B: Condens. Matter Mater. Phys.* **2015**, *92* (9), na.
(26) Usachev, P. A.; Pisarev, R. V.; Balbashov, A. M.; Kimel, A. V.; Kirilyuk, A.; Rasing, T. Optical Properties of Thulium Orthoferrite $TmFeO_3$. *Phys. Solid State* **2005**, *47* (12), 2292−2298.
(27) Watanabe, H.; Kurihara, T.; Kato, T.; Yamaguchi, K.; Suemoto, T. Observation of Long-Lived Coherent Spin Precession in Orthoferrite $ErFeO_3$ Induced by Terahertz Magnetic Fields. *Appl. Phys. Lett.* **2017**, *111* (9), 92401.
(28) Jones, S. P. P.; Gaw, S. M.; Doig, K. I.; Prabhakaran, D.; Hétroy Wheeler, E. M.; Boothroyd, A. T.; Lloyd-Hughes, J. High-Temperature Electromagnons in the Magnetically Induced Multiferroic Cupric Oxide Driven by Intersublattice Exchange. *Nat. Commun.* **2014**, *5*, 3787.

DOI: 10.1021/acsphotonics.7b01402
ACS Photonics XXXX, XXX, XXX−XXX